Lab on a Chip

PAPER

View Article Online
View Journal | View Issue

Cite this: *Lab Chip*, 2024, **24**, 3945

Electric field temporal interference stimulation of neurons *in vitro*†

Annika Ahtiainen, *[a] Lilly Leydolph, [b] Jarno M. A. Tanskanen, [a] Alexander Hunold,[bc] Jens Haueisen [bd] and Jari A. K. Hyttinen [a]

Electrical stimulation (ES) techniques, such as deep brain and transcranial electrical stimulation, have shown promise in alleviating the symptoms of depression and other neurological disorders *in vivo*. A new noninvasive ES method called temporal interference stimulation (TIS), possesses great potential as it can be used to steer the stimulation and possibly selectively modulate different brain regions. To study TIS in a controlled environment, we successfully established an *in vitro* 'TIS on a chip' setup using rat cortical neurons on microelectrode arrays (MEAs) in combination with a current stimulator. We validated the developed TIS system and demonstrated the spatial steerability of the stimulation by direct electric field measurements in the chip setup. We stimulated cultures of rat cortical neurons at 28 days *in vitro* (DIV) by two-channel stimulation delivering 1) TIS at 653 Hz and 643 Hz, resulting in a 10 Hz frequency envelope, 2) low-frequency stimulation (LFS) at 10 Hz and 3) high-frequency stimulation (HFS) at 653 Hz. Unstimulated cultures were used as control/sham. We observed the differences in the electric field strengths during TIS, HFS, and LFS. Moreover, HFS and LFS had the smallest effects on neuronal activity. Instead, TIS elicited neuronal electrophysiological responses, especially 24 hours after stimulation. Our 'TIS on a chip' approach eludicates the applicability of TIS as a method to modulate neuronal electrophysiological activity. The TIS on a chip approach provides spatially steerable stimuli while mitigating the effects of high stimulus fields near the stimulation electrodes. Thus, the approach opens new avenues for stimulation on a chip applications, allowing the study of neuronal responses to gain insights into the potential clinical applications of TIS in treating various brain disorders.

Received 13th March 2024,
Accepted 8th July 2024

DOI: 10.1039/d4lc00224e

rsc.li/loc

1 Introduction

A promising new technique known as temporal interference stimulation (TIS) has been proposed to open up new possibilities in the treatment of neurological and psychiatric conditions. TIS is a non-invasive electrical stimulation (ES) method that promises targeting of neuronal structures at specific depths.[1] Traditional non-invasive brain stimulation methods, such as transcranial magnetic stimulation (TMS) and transcranial electrical current stimulation (tES), have lacked selectivity and effectiveness to therapeutically address target structures at the necessary depth. Hence, the primary option has been invasive deep brain stimulation (DBS), despite its associated risks.[2–4] TIS, however, possesses considerable promise, as it can be steered to affect specific deep regions without modulating the superficial layers of the brain.[1,5] TIS has been demonstrated to have the ability to target deep brain structures and modulate brain functions *in vivo*.[6] TIS has been reported to cause minimal side effects and high tolerability.[7–10] Previously, TIS at theta or gamma frequency envelopes has been used to modulate brain activity in the hippocampus,[6,8,11] striatum,[8,12] and motor cortex,[7,9] demonstrating a targeted stimulation with minimal exposure to overlying brain areas.[6,12] Specifically, theta-frequency TIS has been shown to modulate hippocampal activity, enhance memory performance,[6,11] and alter functional connectivity after TIS.[6] When targeted to the striatum, TIS has been shown to improve motor performance, and modulate the activity in the targeted structures.[12] Another TIS study showed increased neuromodulatory influence between the striatum and motor cortex.[13] In contrast, higher frequency TIS has been shown to facilitate motor learning, while gamma-frequency TIS enhanced motor cortex excitability compared to sham.[7] However, there have been no previous studies of TIS on a

[a] *Faculty of Medicine and Health Technology, Tampere University, 33520, Tampere, Finland. E-mail: annika.ahtiainen@tuni.fi*
[b] *Institute of Biomedical Engineering and Informatics, Technische Universität Ilmenau, 98693, Ilmenau, Germany*
[c] *neuroConn GmbH, 98693, Ilmenau, Germany*
[d] *Department of Neurology, Jena University Hospital, 07747 Jena, Germany*
† Electronic supplementary information (ESI) available. See DOI: https://doi.org/10.1039/d4lc00224e

chip for *in vitro* neuronal systems; thus, our approach potentially offers new ways for studying the effects of TIS and provides methods for neuronal stimulation *in vitro*, especially for lab-on-a-chip approaches.

TIS is realized using two high-frequency sinusoidal currents with different frequencies (*i.e.*, $f_2 > f_1 > 600$ Hz) that, when interfering in the volume conductor, form an interference signal with a low-frequency "envelope" Δf ($\Delta f = f_2 - f_1$), usually between 1 and 100 Hz. As the high-frequency fields are above the frequency range defined by the cell membrane time constant, cells – and neurons – do not react individually to the high frequencies. However, the low-frequency interference field of the resulting beat frequency Δf has the potential to influence neuronal transmembrane potential[14–16] through the nonlinearity of the ion channels charging the membrane capacitance.[17–20] Therefore, TIS has recently drawn attention from researchers as it could offer new ways of modulating the neuronal systems and treating neurological conditions such as Parkinson's disease and chronic pain.[21–27] So far, TIS has been demonstrated using computational studies[23,25,28–31] and *in vivo* applications with rodents[1,32] and human subjects.[6,7,33] However, before our work, TIS had not been tested with *in vitro* cell cultures, where the effects of electrical field interference (EFI) on neuronal cells on chip and their interactions could be assessed more in detail.

In this study, the aim was to establish and assess a new *in vitro* 'TIS on a chip' platform for neuronal cell cultures. The stimulation setup consists of an EFI current stimulator, electrodes for the stimulation, and a microelectrode array (MEA) system, capable of recording and monitoring the resulting stimulus fields and neuronal electrical activity in real time.[34] We validated the developed setup by utilizing different ES paradigms to compare the effects of various stimulation modalities on previously characterized neuronal cultures[35,36] *in vitro*. We investigated how neurons respond to TIS and its low-frequency (LFS) and high-frequency (HFS) counterparts, both in short term and over an extended period. We observed that TIS highly affected the electrophysiological activity of neurons, especially 24 hours after stimulation. Furthermore, we measured the electric field strengths of the stimuli and demonstrated the spatial steerability of TIS in our setup. We showed and validated the usability of our *in vitro* TIS setup, which innovatively integrates electrical current stimulation and electrophysiology recording setup on a chip. Our system provides a new way to assess the modulatory effects of TIS on neuronal electrophysiology, and therefore, to study the potential of TIS in cellular models of therapeutic applications.

2 Experimental section

2.1 Cell culture

2.1.1 Microelectrode array and substrate preparations. MEAs were prepared similarly to Ahtiainen *et al.*[36] Briefly, MEAs (60MEA200/30iR-Ti-gr; Multi Channel Systems MCS GmbH, Germany) were coated with poly-D-lysine (0.05 mg ml^{-1}), rinsed with Dulbecco's phosphate buffered saline (DPBS), air dried, and subsequently coated with laminin (L2020, 20 μg ml^{-1}). MEAs were stored at +4 °C and taken to room temperature (RT) at least 30 minutes before cell plating. Each MEA consisted of 59 recording microelectrodes in an 8 × 8 grid and one internal reference electrode. The microelectrodes were 30 μm in diameter and the electrode spacing was 200 μm. A coating protocol similar to that used for MEAs was applied to μwells (80807; ibidi GmbH, Gräfelfing, Germany) and glass coverslips for live/dead (L/D) assays and immunocytochemistry (ICC), respectively.

2.1.2 Cell plating on MEAs. Rat cortical neurons were plated onto MEAs according to a previously published protocols.[35,36] On the day of plating, neurons (A1084001 or A1084002, Thermo Fisher Scientific) were thawed, their viability was determined with a countess automated cell counter (Thermo Fisher Scientific), and neurons were plated so that each MEA had approximately 80 000 neurons. In the same way, neurons were seeded on coverslips and μwells for further characterization, but the cell counts were $\frac{1}{2}$ or $\frac{1}{4}$ of that was used for MEAs, respectively. Neuron cultures were maintained in neurobasal plus medium with 2% B-12 Plus supplement, 1% P/S, and 1% GlutaMAX supplement (all purchased from Thermo Fisher Scientific). Cells were fed by replacing at least half of the medium three times a week, and always after recording electrical activity. Cell growth and morphology were constantly monitored using a Nikon Eclipse Ts2 (Nikon Corporation, Japan) microscope.

2.1.3 Immunocytochemistry. Immunocytochemistry (ICC) was performed to characterize the cultures at DIV29. The full ICC protocol is available in Ahtiainen *et al.* (2021).[35] The primary antibodies used were glial fibrillary acidic protein (GFAP; AB5804, rabbit, 1 : 1000), microtubule associated protein 2 (MAP2; PA1-10005, chicken, 1 : 1000 or 1 : 2000), postsynaptic density protein 95 (PSD-95; MA1-045, mouse, 1 : 200), and synaptophysin (SYN; MA5-14532, rabbit, 1 : 50). The secondary antibodies used were goat anti-mouse 488 (A32723; 1 : 500), goat anti-Rabbit 555 (A-21428; 1 : 500), and goat anti-chicken 647 (A32933; 1 : 500). All the antibodies were purchased from Thermo Fisher Scientific (Waltham, MA, USA), except for AB5804, which was purchased from Sigma-Aldrich (St. Louis, MO, USA), and all were diluted in 5% (v/v) goat serum (Sigma-Aldrich) in Dulbecco's phosphate-buffered saline (DPBS). Samples were stained with DAPI (4′,6-diamidino-2-phenylindole; D1306, Thermo Fisher Scientific) prior to mounting (10–15 min at RT). Samples were mounted with ProLong™ Gold Antifade Mountant (P10144, Thermo Fisher Scientific; 24 hours in the dark at RT). The coverslips were stored at +4 °C until imaging with an Olympus IX51 fluorescence microscope with an Olympus DP30BW camera (Olympus Corporation, Hamburg, Germany). Fiji (ImageJ, National Institute of Health, USA) software was used to process the images.

2.1.4 Live/dead assay. A live/dead viability/cytotoxicity kit (L3224; Thermo Fisher Scientific) with ethidium

homodimer-1 (4 μM) and calcein-AM (2 μM) was used according to the manufacturer's instructions for cultures in μwells at DIV28. The images were taken using an Olympus IX51 fluorescence microscope and analyzed using a particle size-based analysis similar to that of.[35]

2.2 Stimulation setup and system validation

MEA wells were connected to the DC-STIMULATOR MC (neuroConn GmbH, Germany), which provided the stimulation currents to the culture medium *via* platinum

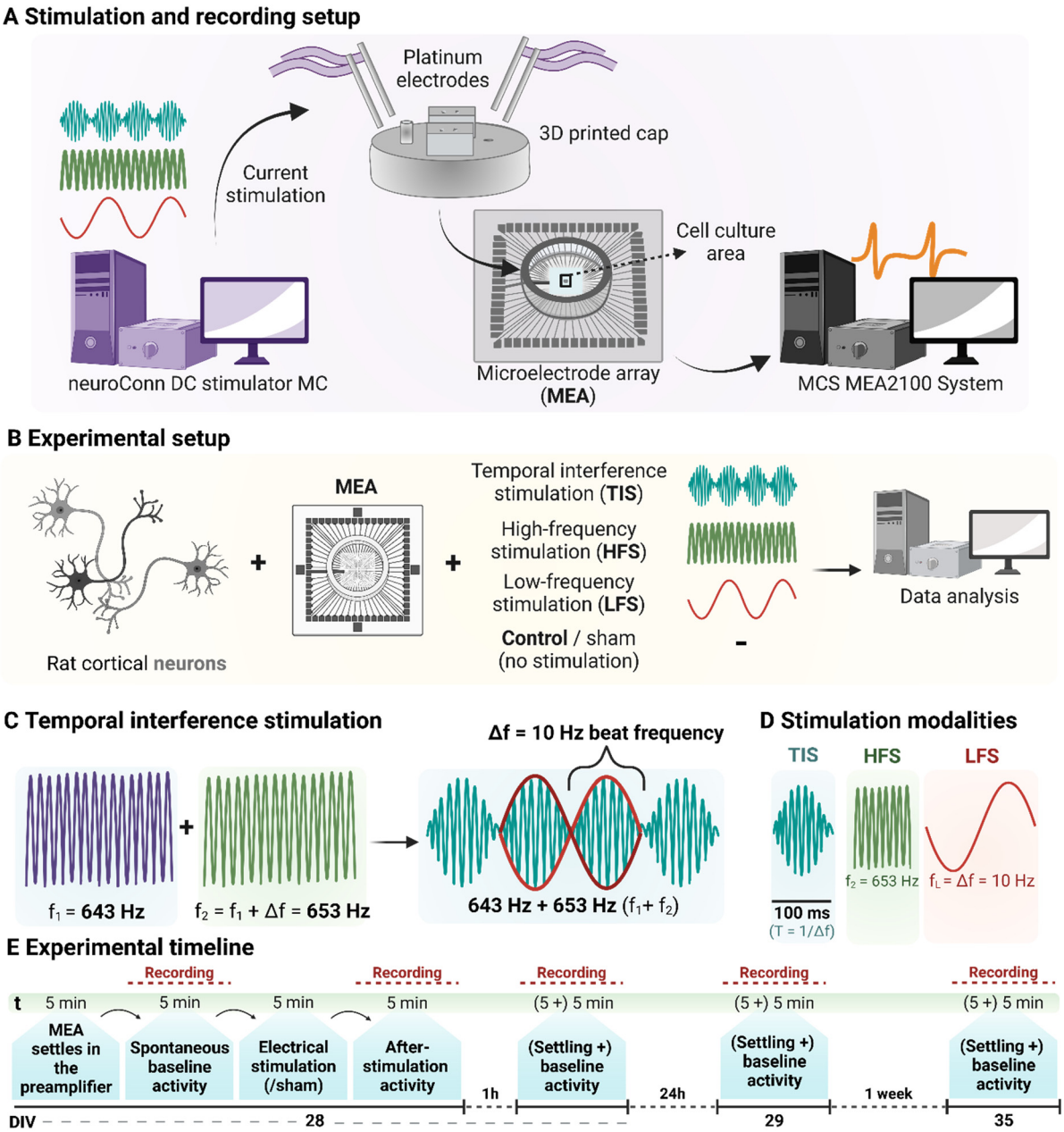

Fig. 1 Principles of the methods used in the study. (A) Neuronal cultures were stimulated using a neuroConn stimulator. The stimulus was conducted *via* platinum rod electrodes submerged in the cell medium in the microelectrode arrays (MEAs). The data were collected using a MEA2100 system from Multi Channel Systems (MCS) GmbH. (B) Rat cortical neurons were plated on MEAs. Neuronal cultures were stimulated with TIS, low-frequency stimulation (LFS), high-frequency stimulation (HFS), and control/sham. (C) The concept of temporal interference stimulation TIS is formed by two different high-frequency signals (f_1 and f_2) that result in a beat frequency Δf with stimulation envelopes corresponding to the LFS signal (10 Hz). (D) Neurons were stimulated continuously for five minutes. The HFS comprised a 653 Hz frequency applied from both stimulation sites. TIS consisted of two high-frequency stimulus currents forming a 10 Hz envelope. LFS comprised a 10 Hz stimulus corresponding to the TIS envelope (representative signal waveforms for TIS and HFS are not shown to scale). (E) At 28 days *in vitro* (DIV), cultures were recorded after five-minute settling and after electrical stimulation (or sham). The activity was recorded immediately after stimulation, and one hour, one day, and one week after stimulation. The signal waveforms of TIS, HFS, and LFS are illustrative representations created with **https://www.Biorender.com**.

electrodes. An illustration of the stimulation and recording setup is shown in Fig. 1A. MEA signals from neurons were recorded prior to, during, and after stimulation with the MEA2100 system (Multi Channel Systems MCS GmbH), which enabled real-time monitoring of the effects of stimulus on neurons. Stimuli were applied *via* four platinum rod electrodes (1 mm × 0.5 mm × 12 mm) through an in-house 3D-printed MEA cap composed of Biomed Amber Resin (Formlabs GmbH, Germany). The cap was printed with a stereolithography 3D printer Form 3B+ (Formlabs GmbH, Germany) and designed using Solidworks 2021 (Dassault Systèmes SolidWorks Corp., France). Various cap designs were tested and validated prior to the final design to establish the desired electric fields. The cap consisted of four elevated holes for inserting the platinum rod electrodes that were submerged in the cell medium. Additionally, the cap had two air holes for a ventilation tube (0.3 mbar; 5% CO_2 + 19% O_2 + 75% N_2). Holes for the platinum rods (1.2 × 0.8 mm) were inserted at a 25° angle to obtain appropriate TIS conductance.

The generated currents for TIS and high frequencies were initially confirmed with measurements using an oscilloscope (MP720665 from Multicomp Pro, Premier Farnell Ltd, USA) (ESI† Fig. S1A and B), as well as thereafter with the MEA2100 system, which was also used during the experiments to record electrical activity of neurons.

The stimulation and recording setups were used to stimulate rat cortical neurons on MEAs (Fig. 1B). We used four different stimulation groups – temporal interference stimulation (TIS), high-frequency stimulation (HFS), low-frequency stimulation (LFS), and control/sham for neurons (n = 16 MEAs; 4 MEAs per group). TIS was realized with two slightly different high-frequency currents (f_1 and f_2) that produced a low beat frequency (Δf), which fell into the range to which neurons could respond (Fig. 1C). To compare the effects of TIS, HFS and LFS with frequencies corresponding to that of TIS, HFS and LFS were also used to stimulate neurons (Fig. 1D; see Section 2.3).

2.3 Stimulation and MEA recordings

The electrical stimulus (TIS/HFS/LFS) was applied for five minutes at 28 days *in vitro* (DIV). The final stimulation parameters were chosen to be 450 μA delivered from both stimulation sites, and a 5 minute stimulation time. These parameter values were selected because they induced relatively high stimulation field amplitudes without being seemingly harmful to the neurons based on a pilot experiment run prior to the full-scale experiment reported herein. Neuronal electrical activity was recorded before stimulation/sham, immediately after, one hour after, 24 hours after, and one week after stimulation/sham (Fig. 1E). MEAs were always allowed to settle in the preamplifier for five minutes before the first recording. For the stimulation, MEAs were not moved from the recording site until the first stimulation was conducted immediately after recording the baseline electrical activity. ES (or sham) was applied for five minutes. For those MEAs that did not receive any stimulation, the stimulation was simulated by keeping the MEAs outside the incubator in the MEA headstage for the same amount of time as those MEAs that were stimulated (TIS/HFS/LFS). After the ES (or sham), at least half of the cell medium was replaced, and MEAs were put back in the incubator. Data were collected and analyzed by comparing the stimulation effects to the percentual change in the control cultures at each time point in question (see Section 2.4.3 for more details). The purpose of using LFS (at $f_L = \Delta f$ = 10 Hz) and HFS (at f_1 = 653 Hz) was to compare these stimulation paradigms alone to enable evaluation of the effects of interference stimulation with respect to control cultures without stimulation. Hence, the stimulation parameters, such as the applied stimulation currents, were kept equal for all stimulation modalities (TIS/HFS/LFS). The stimulation frequencies were selected according to the hardware limitations so that the f_1 and f_2 were the highest possible prime numbers below 700 Hz (hardware bandwidth limit) with a 10 Hz difference. Detailed stimulation paradigms are available in Table 1.

2.4 Data analysis

2.4.1 MEA data. MEA electrophysiological data were recorded at a sampling rate of 50 kHz using the MEA2100-System and Multichannel Experimenter software (both from Multichannel Systems MCS GmbH, Reutlingen, Germany).

Raw electrophysiological data were further analyzed with Matlab 2022a (MathWorks, Inc., Natick, MA, USA) using a previously published, widely used tool for spike sorting,[37] also implemented in.[35] Briefly, a second-order bandpass (300–3000 Hz) elliptic filter with a threshold of $\pm 5\sigma$ (σ = median ($|x|/0.6745$), x = bandpass filtered signal) and 1.5 second detector dead time after each spike was used for sorting. From the sorted, filtered signals, we analyzed the timestamps of neuronal spikes and other parameters of the

Table 1 Stimulation paradigms in the study

	TIS	LFS	HFS	Control
Current (μA)	450	450	450	—
Frequency (Hz)	Channel 1: 653 Channel 2: 643	Channel 1: 10 Channel 2: 10	Channel 1: 653 Channel 2: 653	—
Ventilation during stimulation recordings	+	+	+	+
Days *in vitro* (DIV) for stimulations	28	28	28	28
n (MEAs)	4	4	4	4

electrical activity, such as spike rate, burst rate, burst duration, spikes in bursts, burst spike ratio (BSR%), and interspike interval (ISI) in bursts (details in Table 3). These values were extracted from the data using a tool developed previously in our group.[38,39] Signal traces and impact electrode data (ESI† Fig. S9) were extracted from the analyzed data and plotted with Matlab 2022a.

To observe stimulation electric field strengths, bipolar signals were calculated from the unfiltered MEA data recorded during the different stimulation modalities. Bipolar signals were calculated by subtracting the signals from two adjacent microelectrodes for all microelectrodes (*cf.*, Fig. 2D for the MEA layout) in both horizontal and vertical directions, resulting in two sets of bipolar signals (later denoted as E_x [mV mm^{-1}] and E_y [mV mm^{-1}], respectively). The bipolar signals were converted to field strengths, given the microelectrode distance of 200 μm. The sets of the EFI field strengths for all the used stimulation modalities and the microelectrodes are illustrated in Fig. 3 and S2.†

Power spectral density (PSD) analysis was conducted for the same MEA data used in the stimulation electric field strength analysis. Briefly, PSD and spectrogram analysis were performed on raw unfiltered signals and analyzed for one electrode signal (electrode 44) that was the same for all stimulation modalities. Welch's power spectral density estimates[40] were calculated for the unfiltered and filtered signals. For filtering, an IIR notch filter at a) 653, 643, and 50 Hz (TIS), b) 653 and 50 Hz (HFS), c) 10 and 50 Hz (LFS), and 50 Hz (control/sham) was applied and plotted with Matlab 2022a. The PSD and spectrogram results for all the used stimulation modalities are illustrated in Fig. 4 and S3–S6.†

2.4.2 Connectivity analysis. Correlated spectral entropy (CorSE) analysis was used to evaluate the connectivity strengths in the networks. CorSE uses correlations of time-varying spectral entropies between all MEA channels to evaluate synchronicity. The connectivity strength between MEA electrodes is established by their magnitude of correlation, and the overall average connection strength considers all the electrode pairs in the network. The analysis was done according to Kapucu *et al.*,[41] using Matlab 2022a with a connection threshold of 0.75. CorSE was analyzed at DIV28 and DIV29 (24 hours after the stimulation/sham).

2.4.3 Statistical analysis. All statistical analysis was done with Graphpad Prism (v.9.0). Significance values below 0.05 were considered significant. The neuronal maturation data was analyzed using the one-way analysis of variance (ANOVA) followed by Tukey's multiple comparisons test for corrections of the adjusted *p*-values. Two-way ANOVA followed by Šídák's multiple comparisons test for corrections (ESI† Fig. S9) was used for the 'middle' and 'edge' electrode comparisons (α = 0.05; adjusted *p*-values: ns = not significant, $*p < 0.05$, $**p < 0.01$, $***p < 0.001$). The electrical stimulation (TIS/HFS/LFS/control) data had a non-normal distribution that was confirmed using Shapiro–Wilk test. Therefore, the data was statistically tested using nonparametric Mann–Whitney U test. For the effects of ES (% of control), the results were obtained by comparing the changes in each group with the respective changes in the control group at the time of the recording. Hence, the percentual changes were obtained by comparing the changes caused by the stimulation to the respective changes in the control cultures occurring at each time point. Asterisks in the Fig. 6 indicate the level of significance, where * denotes $p < 0.05$, and *ns* not significant. All statistical details are available in the ESI† (Tables S1–S4).

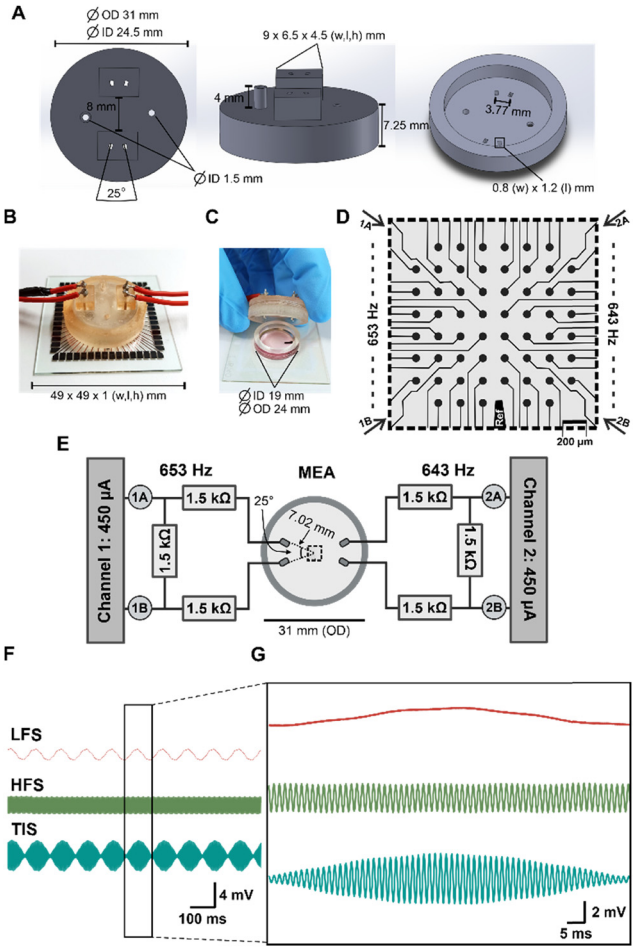

Fig. 2 Electrical stimulation system and the recorded stimulus waveforms. (A) The measures and design of the 3D printed cap (B and C) on microelectrode array. (D) MEA electrode area. Microelectrodes are depicted in dark gray circles, and the reference electrode is indicated as a black bar. The distance between each microelectrode is 200 μm, and the electrode diameter is 30 μm. (E) Schematic of the experimental setup, including Ich_1 = Ich_2 = 450 μA with 1.5 kΩ resistors. A microelectrode array was located in between the two channels, and the stimulus reached the MEA at a 25° angle. (F) 1 second recordings of the low-frequency stimulation (LFS), high-frequency stimulation (HFS), and temporal interference stimulation (TIS) on the MEAs. (G) 100 ms close-ups from each of the stimulations (HFS/LFS/TIS).

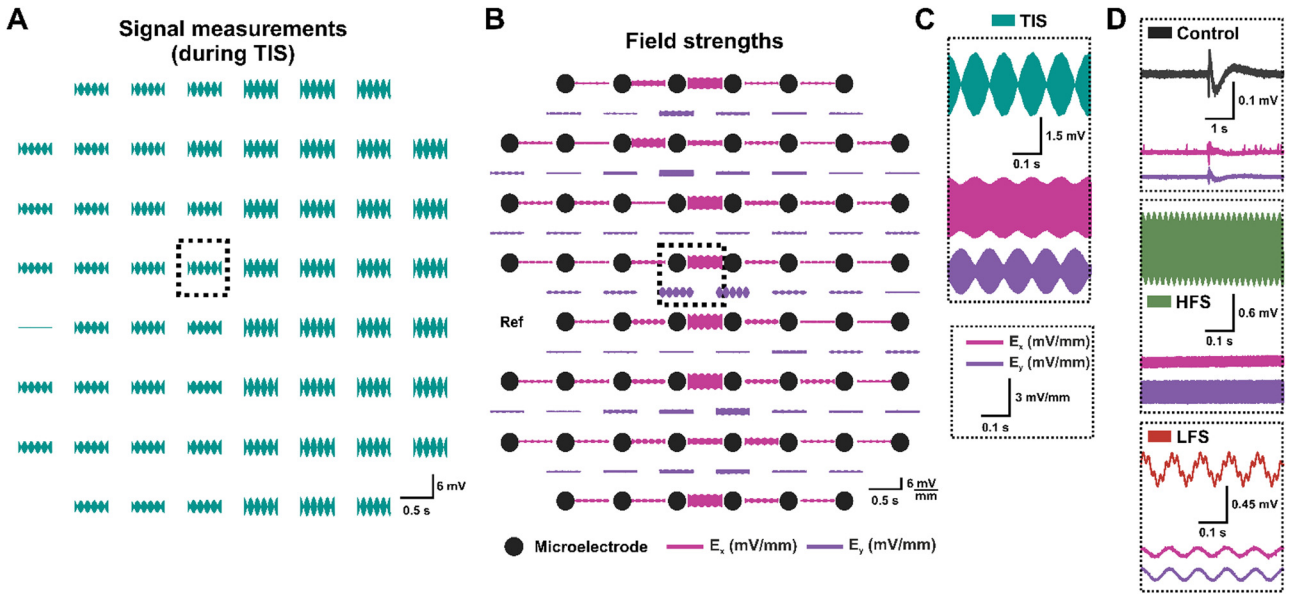

Fig. 3 Electrical stimulation system, recorded stimulus waveforms, and electric field strengths during the stimulation. (A) Signal traces of TI-stimulated culture (during stimulation). (B) The electric field strengths (indicated with pink and purple traces) between two adjacent electrodes in both horizontal and vertical directions (E_x [mV mm^{-1}] and E_y [mV mm^{-1}], respectively). For TIS, both electric field strengths were lower at the edges of the electrode area and highest in the middle of it, which would support steerability of our TIS system. The microelectrodes are depicted as dark gray circles. (C) A close-up of the signals depicted in A and B from electrode 44. (D) Close-ups of the signal traces and electric field strengths (*x* and *y* directions, depicted with pink and purple traces, respectively) for control, HFS, and LFS cultures from the same electrode as in (C) during stimulation (ID 44) (unfiltered data).

3 Results and discussion

3.1 Electrical stimulation concept and validation on microelectrode arrays

We established an *in vitro* stimulation and recording setup by combining a current stimulator with a MEA system that can record neuronal electrical activity. The stimulus was conducted *via* platinum rod electrodes to cells located on the MEA electrode area. Fig. 2A–C shows the design of the 3D-printed cap through which the platinum electrodes were inserted. The directions from the platinum electrodes to the MEA area (with the neurons) is illustrated in Fig. 2D. Fig. 2E illustrates the schematics of the TIS setup with two electrode pairs fed with currents of 450 μA.

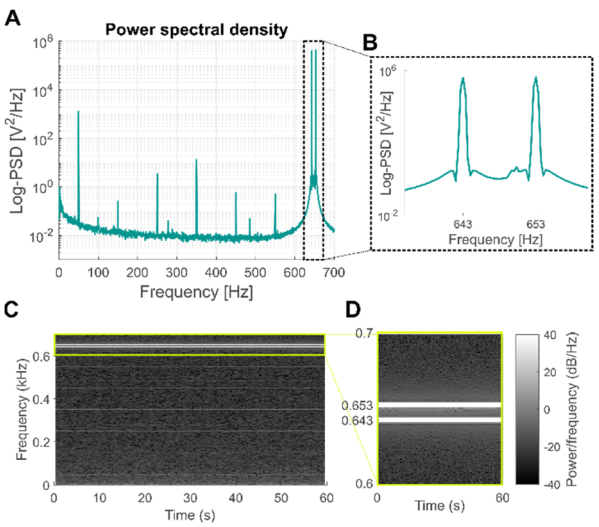

Fig. 4 (A) A power spectral density (PSD) analysis from unfiltered data during temporal interference stimulation (TIS). (B) Close-up of (A). (C) Spectrogram of unfiltered TIS signal during stimulation with the stimulation frequencies clearly visible and remained consistent throughout the stimulation. (D) Close-up of (C). In all cases, the data is derived from one respective electrode locating in the middle of the electrode area that was used to generate the images.

Prior to stimulation of cells, the stimulation system that comprised of the stimulator and the MEA recording system was verified without any cell cultures. Using only the cell culture medium, all stimulations (TIS, HFS, and LFS) were observed in the MEA2100 recordings (Fig. 2F). Fig. 2G shows 100 ms close-ups of each of the stimulations. The LFS had the lowest frequency at 10 Hz, the HFS had high-frequency characteristics at 653 Hz, and the TIS had 10 Hz envelopes, along with the high-frequency signals within the envelopes, as expected.

Next, we evaluated and validated the system with cell cultures; Fig. 3A shows the entire MEA electrode area of one representative TI-stimulated neuronal culture. Depending on the electrode in question, the TIS amplitudes were substantially higher, especially compared to control and LF-stimulated cultures (Table 2). The recorded TIS amplitude was the lowest around the reference electrode (electrode number 15), which was also internally grounded in the system. The amplitudes were the highest further away from the reference electrode.

As the field potentials in MEA are recorded against a common reference electrode (electrode number 15), we also calculated the local electric field strengths in both horizontal

Table 2 Minimum and maximum amplitude values, average minimum and maximum amplitudes (±standard deviation [SD]) and the respective minimum and maximum electric field strengths (mV mm^{-1}) across all the electrodes for representative neuronal cultures on MEAs during sham, TIS, HFS, and LFS stimulations (E_x = horizontal electric field strength, E_y = vertical electric field strength [mV mm^{-1}])

	Minimum values; mean ± SD			Maximum values; mean ± SD		
	Voltage (mV)	E_x (mV mm^{-1})	E_y (mV mm^{-1})	Voltage (mV)	E_x (mV mm^{-1})	E_y (mV mm^{-1})
Ctrl	−0.4; −0.1 ± 0.1	−2.0; −0.9 ± 0.5	−2.1; −0.9 ± 0.5	0.4; 0.1 ± 0.1	2.2; 0.9 ± 0.5	2.1; 0.9 ± 0.5
TIS	−2.7; −2.0 ± 0.5	−5.9; −1.8 ± 1.2	−4.1; −1.4 ± 0.7	2.7; 2.0 ± 0.5	5.7; 1.8 ± 1.2	4.5; 1.4 ± 0.8
HFS	−1.2; −0.7 ± 0.2	−3.1; −1.1 ± 0.8	−3.3; −1.1 ± 0.7	1.0; 0.7 ± 0.2	4.7; 1.0 ± 0.8	2.8; 1.0 ± 0.7
LFS	−0.9; −0.3 ± 0.1	−2.2; −1.0 ± 0.5	−2.9; −1.0 ± 0.5	0.6; 0.3 ± 0.1	3.7; 1.2 ± 0.6	3.6; 1.1 ± 0.6

and vertical directions (E_x [mV mm^{-1}] and E_y [mV mm^{-1}], respectively) for control, TIS, HFS, and LFS-stimulated cultures on MEA. The calculated field strengths during TIS are shown in Fig. 3B and the other stimulation modalities (HFS, LFS, control/sham) can be found in ESI† Fig. S2. For the TIS-stimulated MEA, the electric field strengths also varied within the electrode area, being the highest in the middle of the electrode area in both vertical and horizontal directions and lowest at the edges of the electrode area (Fig. 3B). Specifically, amongst the 59 electrodes and different field directions considered, the local interference electric field strengths were highest between the electrode pairs in the middle of the electrode array in both horizontal and vertical directions – a result fitting nicely with the theoretical consideration of the EFI. For the other stimulation modalities, the local electric field strengths were lower compared to TIS (Fig. 3C, D and Table 2). TIS promises selective targeting of different spatial areas of neural populations, while at the same time minimizing off-target effects.[1,42–44] Notably, our findings indicate a spatial selectivity of the introduced TIS system, thus potentially facilitating targeting specific stimulation areas. Contrarily, with conventional stimulation methods, the local electric field strengths are the highest in proximity to the stimulation electrodes.[45,46] Our results highlight the potential of TIS to produce high local electrical interference fields further away from the stimulus electrodes. Hence, our results indicate that TIS can open new prospects for spatially targeted ES applications not only *in vivo* but also *in vitro*.

We also validated the setup by characterizing TIS signal power content over frequency (power spectral density [PSD]). Notably, the stimulation frequencies of f_1 = 653 Hz and f_2 = 643 Hz were clearly visible in the unfiltered signal that was recorded during stimulation (Fig. 4A and B). Also, the spectrogram analysis that reveals the spectrum of frequencies over time demonstrated clear bands for the stimulation frequencies (f_1 and f_2) during the entire stimulation (Fig. 4C and D). The corresponding results for the other stimulation modalities (HFS, LFS, and control/sham) are available in ESI† Fig. S3–S6.

3.2 Neuronal cell cultures

Primary rat cortex neurons were used to assess the impact of TIS on neurons. Neuronal cultures were followed for 35 days on MEAs (representative images of the cultures at DIV28 in Fig. 5A). Fig. 5B and C shows the representative signal traces of neurons at DIV28.

The electrical activity of the cultures was evaluated weekly, starting with DIV7. The assessed electrophysiological features and their descriptions are listed in Table 3. All statistical tests and details of the maturation of the cultures can be found in ESI† Table S1. The spike rates and burst rates rose steadily until DIV35 for all the cultures, as expected (Fig. 5D and E). The burst duration shortened toward DIV35 but remained statistically unchanged (Fig. 5F). Also, the number of spikes in bursts reduced toward DIV35 and was significantly higher at DIV21 than DIV7 (Fig. 5G). The ratio of spikes involved in bursts (BSR) was lower at DIV7 but rose rapidly already from DIV14 (Fig. 5H). The interspike interval (ISI) in bursts was the highest at DIV7 and decreased significantly for DIV14, 21, 28, and 35 (Fig. 5I). The number of active electrodes was still 59 at DIV35, except for one MEA (ESI† Fig. S1C). Furthermore, the connectivity of the neuronal cultures was evaluated with correlation spectral entropy (CorSE) analysis. In general, the cultures had a high neuronal network connectivity across the MEA area (0.62 ± 0.16 out of 1; Fig. 5J).

The viability of the cultures was analyzed at DIV28. The cultures had very few dead cells (viability 83 ± 10%, ESI† Fig. S1D). Furthermore, at DIV29, cultures were stained with immunocytochemistry (ICC), and the cultures expressed their typical neuronal and astrocytic proteins, as expected (Fig. 5K). Moreover, pre- and postsynaptic proteins, indicated by synaptophysin (SYN) and postsynaptic density protein-95 (PSD-95), were present, further implying functional connections between the neurites in the cultures (Fig. 5L). The electrophysiological properties and other characteristics of the cultures, such as cell composition and morphology, resembled those in our previous studies using the same cells.[35,36] The neurons exhibited a relatively high electrophysiological activity, similarly to what we have previously observed.[36] Hence, the neuronal cultures exhibited their typical electrophysiological and morphological features; the functional networks exhibited robust spiking and bursting activities, as also observed previously by others.[47,48]

3.3 Electrical stimulation of neurons *in vitro*

At DIV28, neurons were subjected to ES or sham for five minutes (n = 4 MEAs/group, as described in Fig. 1). All statistical

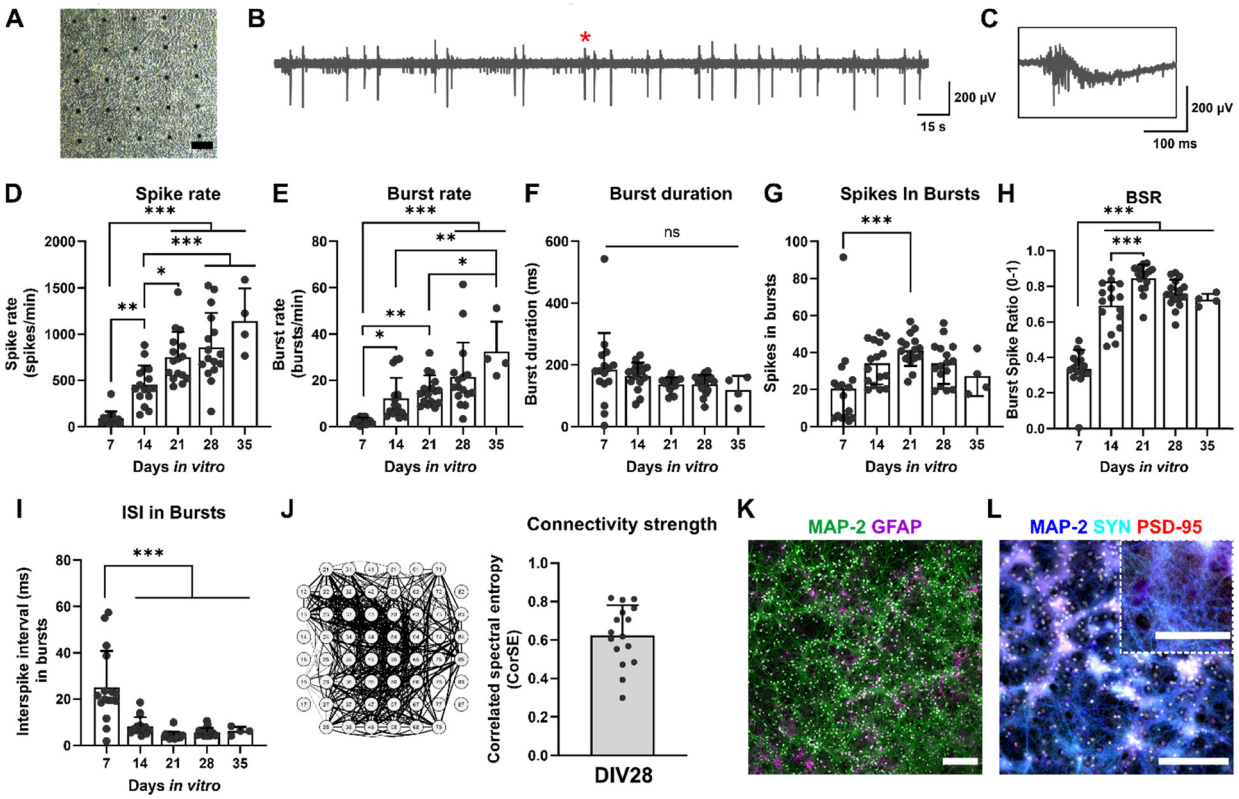

Fig. 5 Characterization of the neuronal cultures. (A) A brightfield image of a neuronal culture on MEA at DIV28. The scale bar is 100 µm. The black dots are the microelectrodes on the MEA surface. (B and C) Representative signal traces of neurons at DIV28. The red star indicates the spot of the 300 ms close-up in C. (D–I) Electrophysiological characteristics of the cultures during five weeks *in vitro*. In general, neurons had higher electrical activity during the last weeks of culture with no differences in burst duration during the culture period. (J) Correlation spectral entropy (CorSE) analysis of the functional connectivity of neurons at DIV28. (K) Immunocytochemical (ICC) images of neurons (MAP2, microtubule associated protein 2) and astrocytes (GFAP, glial fibrillary acidic protein) at DIV29. Nucleus staining DAPI (4′,6-diamidino-2-phenylindole) is indicated in white. The scale bar is 200 µm. (L) ICC images of neurons (MAP2) and pre- and postsynaptic proteins (SYN, synaptophysin; PSD-95, postsynaptic density protein-95, respectively) at DIV29. Nucleus staining DAPI is indicated in white. The scale bar is 200 µm, and 100 µm for the close-up. All statistical comparisons were done using one-way ANOVA followed by Tukey's multiple comparisons test. Adjusted *p*-values are indicated as ns = not significant, $*p < 0.05$, $**p < 0.01$, $***p < 0.001$ (n = 16 MEAs, except for DIV35 n = 4 MEAs).

Table 3 The assessed electrophysiological features of the cultures and their descriptions

Electrophysiological features	Description	Unit/scale
Number of active electrodes	The number of active electrodes in MEA. An electrode is considered active if it has ≥10 spikes per min (otherwise excluded from the analysis)	0–60
Spike rate	Number of spikes per minute (spike detection threshold ±5σ)	1 min^{-1}
Burst rate	Number of bursts per minute. Burst consists of ≥3 spikes	1 min^{-1}
Burst duration	The average duration of a burst	ms
Spikes in bursts	The average number of spikes in bursts	≥0
Burst spike ratio (BSR%)	Percentage of spikes involved in bursts	0–1 (1 = 100%)
Interspike interval (ISI) in bursts	Average time between sequential spikes in bursts	ms
Correlated spectral entropy (CorSE)	Evaluates MEA signal synchronicity by calculating the correlations of time-varying spectral entropies between the MEA channels (connection threshold ≥0.75)	0–1

tests with details can be found in ESI† Tables S2–S4. Prior to electrical stimulation, all the cultures exhibited very similar activity except for the HFS cultures, which had slightly elevated spike rates (+34%, p = 0.0286; Mann–Whitney U test) and smaller BSRs than control (−8%, p = 0.0286) (Fig. 6A and E). Moreover, neurons were electrically active also during TIS, which was revealed after filtering the stimulation frequencies from the measured neuronal signals (ESI† Fig. S4). However, the spiking activity was lower during stimulation compared to baseline activity measured before the stimulation.

Directly after the five-minute stimulation, LFS cultures experienced decreased spike rates (−26%), burst rates (−52%),

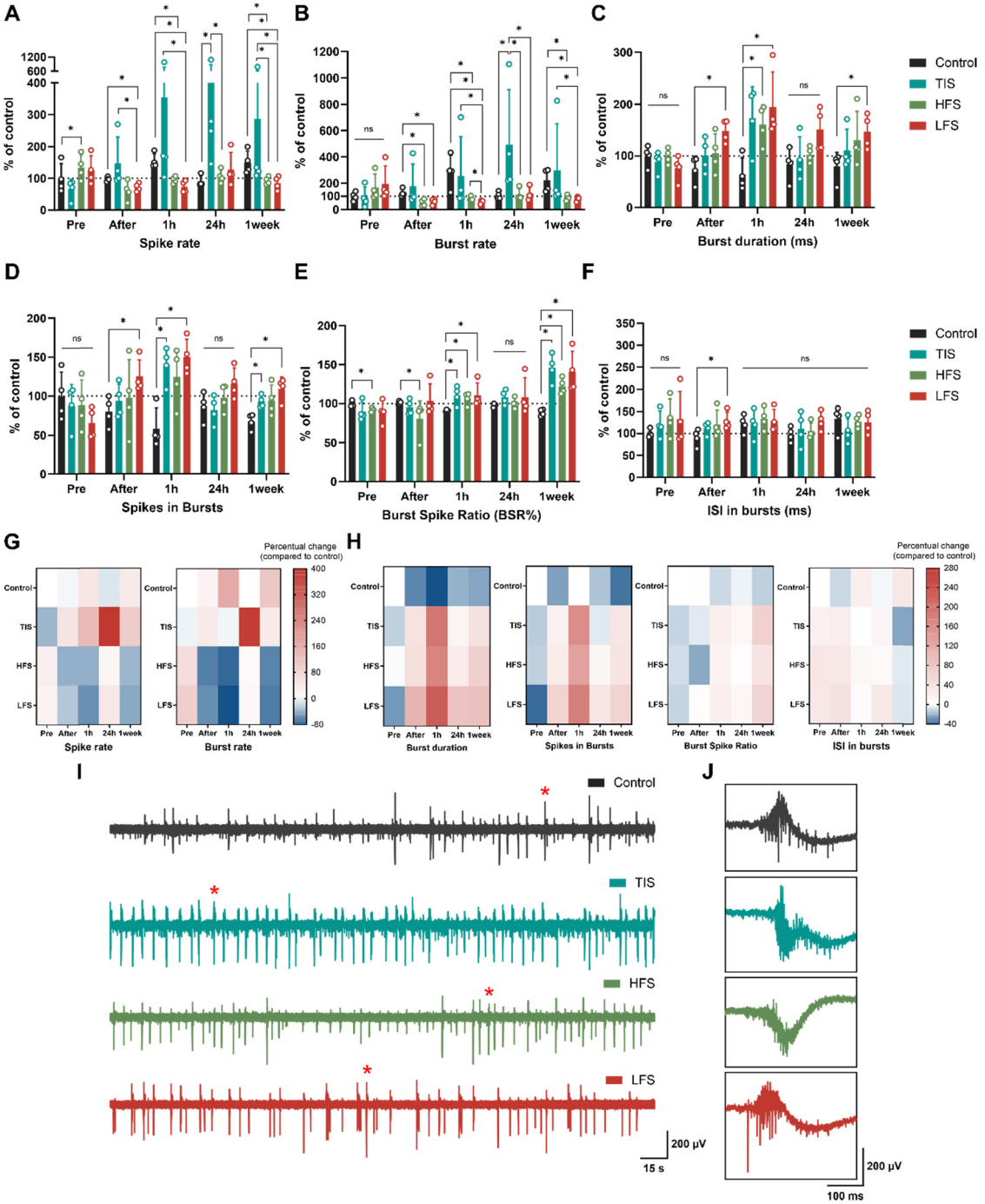

Fig. 6 Electrophysiology of neuron cultures. (A–F) The effects of ES were compared to changes in control cultures at each time point. TIS (653 + 643 Hz with 10 Hz beat frequency) affected spike and burst rates by increasing the electrophysiological activity, especially after 24 hours. The effects of HFS (653 Hz) and LFS (10 Hz) were the most prominent one hour after the stimulation, as the spike and burst activities were suppressed and the duration of bursts prolonged. The burst spike ratio (BSR%) was increased for all ES types one hour after the stimulation, as were spikes in bursts for TIS and LFS. Some of the effects observed in spike rates and BSRs were observed even one week after the stimulation for TIS, HFS, and LFS. Bar graphs show means ± SD with data points. (G and H) Heatmaps of the percentual increases and decreases compared to the control/sham cultures. Control values before stimulation were adjusted to 0 (indicating no change) and values below that show decreases and values above 0 show increases in the respective activity parameters. (I and J) Representative signal traces of control, TI, HF, and LF-stimulated neurons 24 hours after the stimulation and their 300 ms cut-outs, indicated with red stars in the full signals. ns = not significant, $*p < 0.05$ (n = 4 MEAs/condition. All statistical tests were done using the Mann–Whitney U test).

elevated burst duration (+105%), number of spikes in bursts (+61%), and ISI (+41%) compared to control cultures (Fig. 6A–D and F; $p = 0.0286$ for all). As expected, HFS did not affect the neurons as much as the LFS, but the HFS cultures had

decreased burst rates (−59%) and BSR (−20%) compared to control cultures right after the stimulation (Fig. 6B and E; p = 0.0286). Furthermore, one hour after stimulation, LFS and HFS showed decreased spiking (−51% and −37%, respectively), and bursting (−80% and −70%, respectively), increased burst duration (+227 for LFS and 171% for HFS) and BSRs (+22% for LFS and +17% for HFS), and an increased number of spikes in bursts (+178%) for the LFS (p = 0.0286 for all). Moreover, TIS cultures had an elevated number of spikes in bursts (+159%) and BSR (+22%) one hour after the stimulation compared to the control cultures (p = 0.0286), and the differences were emphasized the next day.

Twenty-four hours after the stimulation, TIS cultures had significantly increased spike rates and burst rates by +397% and +389%, respectively (Fig. 6A, B and G; p = 0.0286 for both). There were no differences in electrical activity for the LFS and HFS cultures after 24 hours compared to control cultures, but the differences in spike rates and burst rates were significant compared to TI-stimulated cultures (p = 0.0286). This result is also in line with a previous *in vivo* study that reported hippocampal TIS to improve associative memory 24 hours after stimulation, but not earlier, after 90 minutes (Δf = 5 Hz).[11] Burst durations, spikes in bursts, BSRs, and ISI in bursts remained unchanged for all the stimulation conditions 24 hours after the stimulation (Fig. 6C–F and H).

Cultures were also assessed one week after the stimulation, and LFS and HFS cultures still showed decreased spike (−40% and −34%, respectively) and burst rates (−61% and −57%, respectively) compared to control and TI-stimulated cultures (p = 0.0286 for all). Also, burst duration was higher (+86%) for the LFS, as were the number of spikes in bursts and BSR (+60% and 58%, respectively, p = 0.0286). Furthermore, TI-stimulated cultures showed elevated numbers of spikes in bursts and increased BSRs one week after the stimulation compared to control cultures (+36% and +64%, p = 0.0286). The ISI in bursts remained unchanged for all one week after the stimulation (Fig. 6F).

Taken together, TI-stimulation was the only form of ES applied that elicited the neuronal electrophysiological activity as seen in increased spiking and bursting activity after the stimulation (Table 4). The temporally interfering electrical fields increased the neuronal electrical activity, and the trend was already visible one hour after the stimulation, but the effect was emphasized 24 hours after the stimulation. On the contrary, the "conventional" LFS suppressed neuronal electrical activity instead of eliciting it. This suppressing effect was evident immediately after stimulation and lasted up to a week. The HFS had less impact on the neuronal cultures, but seemed to impede electrical activity, especially one hour and one week after the applied stimulus. The percentual changes compared to the changes in the control cultures are depicted in Fig. 6G for the spike rates and burst rates and in Fig. 6H for the rest of the parameters. All stimulation results are summarized in Table 4.

The representative signal traces 24 hours after the stimulation for all the culture conditions are presented in Fig. 6I and J. Moreover, the functional connectivity changes 24 hours after the stimulation, when the effects were the most prominent, were evaluated using CorSE analysis. ESI† Fig. S7 represents the CorSE figure of a representative MEA of each group 24 hours after the stimulation and the results of the analysis. The connectivity results indicated that none of the stimulation methods affected the connectivity strengths of the cultures despite the changes in neuronal spiking and bursting, especially due to the TIS. Representative raster plots for each stimulation modality are presented in ESI† Fig. S8.

Table 4 Percentual differences compared to the control/sham at each time point. Control values (before stimulation) were adjusted to 0, indicating no change. Values below 0 show decreases and values above 0 show increases in the respective activity parameters compared to control cultures (n = 4 MEAs/condition; Mann–Whitney U test; ns = not significant, *p = 0.0286)

		Control	TIS		HFS		LFS	
	Time point	%	%	p	%	p	%	p
Spike rate	After	−4	53	ns	−37	ns	−26	*
	+1 h	50	136	ns	−37	*	−51	*
	+24 h	−12	397	*	20	ns	45	ns
	+1 week	41	102	ns	−34	*	−40	*
Burst rate	After	25	41	ns	−59	*	−52	*
	+1 h	170	−5	ns	−70	*	−80	*
	+24 h	1	389	*	12	ns	17	ns
	+1 week	111	42	ns	−57	*	−61	*
Burst duration	After	−28	40	ns	45	ns	105	*
	+1 h	−40	192	ns	171	*	227	*
	+24 h	−18	15	ns	26	ns	84	ns
	+1 week	−21	41	ns	66	ns	86	*
Spikes in bursts	After	−22	21	ns	26	ns	61	*
	+1 h	−46	159	*	131	ns	178	*
	+24 h	−14	−5	ns	14	ns	35	ns
	+1 week	−32	36	*	38	ns	60	*
BSR%	After	1	−5	ns	−20	*	3	ns
	+1 h	−9	22	*	17	*	22	*
	+24 h	−3	11	ns	3	ns	11	ns
	+1 week	−11	64	*	38	*	58	*
ISI in bursts	After	−9	23	ns	32	ns	41	*
	+1 h	22	0	ns	10	ns	5	ns
	+24 h	−2	13	ns	8	ns	31	ns
	+1 week	33	−21	ns	−5	ns	−6	ns

The reasons for the observed impact in neuronal cultures are multifaceted – starting with the parameters of the stimulation, including the applied stimulation current and duration. Most brain stimulation studies, including the original study by Grossmann *et al.*,[1] use a 20 minute stimulation time, as it has been shown to induce direct effects and aftereffects in electroencephalograms (EEGs).[49,50] Moreover, in recent *in vivo* studies, longer stimulation times, ranging from ten minutes to over half an hour, have been applied.[6,9,12] However, these long stimulation durations were not feasible in our study setup, as our purpose was to demonstrate the TIS *in vitro* setup and the effects of short stimulation. Whereas a number of TIS studies have reported clear effects in certain applications, *e.g.*, Piao *et al.*[9] found no significant effects. Our setup will open future research possibilities to assess TIS in a controlled *in vitro* environment. Using our *in vitro* tools, future studies can now assess different cell targets, stimulation envelopes, and carrier

frequencies that have been applied *in vivo*.[6,8–12] Due to present hardware limitations, we were not able to replicate the Grossman setup[1] with respect to the carrier frequency. It would be helpful to systematically investigate the influence of different carrier frequencies. However, our results suggest that the frequency limitation of our stimulator was not significant for our conclusions and demonstrate the applicability of TIS at the utilized carrier frequencies. Our *in vitro* 'TIS on a chip' setup would open new avenues to explore the mechanisms of various stimulus parameters, including stimulus frequency combinations.

As hypothesized in the TIS theory, HFS at 653 Hz did not evoke increased electrophysiological responses in neurons, nor did the LFS at 10 Hz. Instead, HFS and LFS seemed to suppress neuronal spiking and bursting activity, and this suppressive effect seemed to persist even one week after stimulation. This suggests that LFS and HFS may have affected neurons, for example, by changing their excitability through long-term depression or potentiation and alterations in synaptic plasticity.[51] Furthermore, previous research suggests that the effects of HFS and LFS on neuronal activity are highly dependent on the specific stimulus site and parameters but that they could suppress epileptiform activity.[52–55] Moreover, emerging evidence suggests that high-frequency conduction blocks might block or inhibit the propagation of action potentials along axons, thereby contributing to the observed effects.[23] However, it is noteworthy to acknowledge that, in general, the ES parameters used, aspects of the experimental setup such as invasiveness, and consequently the results usually vary highly across studies, both *in vitro* and *in vivo*.

We also evaluated whether the different stimulation modalities affected neurons differently depending on their location on the microelectrode area. The spike rates for the individual electrodes were analyzed in a similar manner to Section 3.3. The spatial analysis revealed consistent results – the electrophysiological spiking activity of neurons increased 24 hours after TIS (ESI† Fig. S9A). However, there were no significant spatial differences observed between the middle (n = 16 electrodes) and edge (n = 43 electrodes) electrodes in any (TIS/HFS/LFS/control) of the stimulated cultures (ESI† Fig. S9B). This observed network-wide TIS impact is influenced by dynamic interactions, synaptic strengths, functional connectivity, and action potential propagation in the cortical network, all of which contribute to the activation of neurons across the whole culture area.[56–58] Moreover, as shown in Section 3.3, the effects of TIS are long-lasting, suggesting sustained modulation of neuronal activity over time and across the cell neuronal culture. Therefore, further investigation and a larger microelectrode surface area may be needed to elucidate the precise spatiotemporal effects of TI-stimulation *in vitro*.

4 Conclusions

Temporal interference stimulation (TIS) utilizes slightly differing frequencies that superimpose spatially and temporally to create a low-frequency beating amplitude electric field. In this study, we introduced an experimental *in vitro* setup that enabled us to explore the effects of TIS on neuronal electrophysiology at the cellular and network levels. We successfully established, verified, and validated the 'TIS on a chip' setup for non-invasive stimulation of neurons with and without cell cultures. Using direct MEA electrode voltage measurements, we demonstrated the capability of TIS to provide spatially targetable stimulation fields *in vitro*. Moreover, employing neuronal cultures on MEAs, we observed pronounced effects of TIS on these cultures, resulting in a prominent electrophysiological response. TIS on a chip approach holds promise for assessing the interactions between neural cells and *in vitro* controlled EFI stimulation for brain modulation purposes. TIS offers better spatial control over the stimulation while minimizing unwanted effects on non-targeted brain regions, thus making it an attractive subject of study for future stimulation methods both *in vitro* and *in vivo*. Our study provides insight into the modulatory effects of different stimulation systems and their influence on neuronal electrophysiology. Our *in vitro* 'TIS on a chip' application enables spatiotemporal control over the modulation of stimulation fields, thereby providing a demonstration of using TIS on a chip to gain a deeper understanding of the mechanism and applicability of TIS *in vivo*.

Data availability

ESI† is available for this paper. Datasets are available on request: the raw data supporting the conclusions of this article will be made available by the authors upon a reasonable request. Correspondence and requests for materials should be addressed to annika.ahtiainen@tuni.fi. All original MATLAB codes used in the paper are publicly available.

Author contributions

Conceptualization: J. A. K. H., J. H., A. H., A. A.; data curation: A. A., L. L.; formal analysis: A. A.; funding acquisition: J. A. K. H., J. H.; investigation: A. A., L. L.; methodology: A. A., L. L.; project administration: J. A. K. H., J. H., J. M. A. T.; resources: J. A. K. H., J. M. A. T., J. H., A. H.; software: A. A., J. M. A. T.; supervision: J. A. K. H, J. H.; validation: A. H., J. A. K. H., J. H., J. M. A. T., A. A., L. L.; visualization: A. A.; writing – original draft: A. A.; writing – review & editing: J. A. K. H., J. M. A. T., J. H., A. H., A. A.

Conflicts of interest

A. H. is partially employed with neuroConn GmbH. Otherwise, the authors declare no conflict of interest.

Acknowledgements

The authors acknowledge the doctoral school of Faculty of Medicine and Health Technology, Tampere University, for supporting the work of A. A. and the Tampere Imaging

Facility for their services. The authors acknowledge the Academy of Finland – funded Centre of Excellence in Body-On-Chip Research (grant number 353178) for supporting laboratory equipment. Otherwise, this research did not receive any specific grant from funding agencies in the public, commercial, or not-for-profit sectors.

Notes and references

1 N. Grossman, D. Bono, N. Dedic, S. B. Kodandaramaiah, A. Rudenko, H.-J. Suk, A. M. Cassara, E. Neufeld, N. Kuster, L.-H. Tsai, A. Pascual-Leone and E. S. Boyden, *Cell*, 2017, **169**, 1029–1041.e16.
2 J. K. Krauss, N. Lipsman, T. Aziz, A. Boutet, P. Brown, J. W. Chang, B. Davidson, W. M. Grill, M. I. Hariz, A. Horn, M. Schulder, A. Mammis, P. A. Tass, J. Volkmann and A. M. Lozano, *Nat. Rev. Neurol.*, 2021, **17**, 75–87.
3 A. M. Lozano, N. Lipsman, H. Bergman, P. Brown, S. Chabardes, J. W. Chang, K. Matthews, C. C. McIntyre, T. E. Schlaepfer, M. Schulder, Y. Temel, J. Volkmann and J. K. Krauss, *Nat. Rev. Neurol.*, 2019, **15**, 148–160.
4 A. Videnovic and L. V. Metman, *Mov. Disord.*, 2008, **23**, 343–349.
5 J. Dmochowski and M. Bikson, *Cell*, 2017, **169**, 977–978.
6 I. R. Violante, K. Alania, A. M. Cassarà, E. Neufeld, E. Acerbo, R. Carron, A. Williamson, D. L. Kurtin, E. Rhodes, A. Hampshire, N. Kuster, E. S. Boyden, A. Pascual-Leone and N. Grossman, *Nat. Neurosci.*, 2023, **26**(11), 1994–2004.
7 R. Ma, X. Xia, W. Zhang, Z. Lu, Q. Wu, J. Cui, H. Song, C. Fan, X. Chen, R. Zha, J. Wei, G.-J. Ji, X. Wang, B. Qiu and X. Zhang, *Front. Neurosci.*, 2022, **15**, 800436.
8 P. Vassiliadis, E. Stiennon, F. Windel, M. J. Wessel, E. Beanato and F. C. Hummel, *J. Neural Eng.*, 2024, **21**, 024001.
9 Y. Piao, R. Ma, Y. Weng, C. Fan, X. Xia, W. Zhang, G. Q. Zeng, Y. Wang, Z. Lu, J. Cui, X. Wang, L. Gao, B. Qiu and X. Zhang, *Brain Sci.*, 2022, **12**, 1194.
10 Y. Zhang, Z. Zhou, J. Zhou, Z. Qian, J. Lü, L. Li and Y. Liu, *Front. Hum. Neurosci.*, 2022, **16**, 918470.
11 T. Popa, E. Beanato, M. J. Wessel, P. Menoud, F. Windel, P. Vassiliadis, I. R. Violante, K. Alania, P. Dzialecka, N. Grossman, E. Neufeld and F. C. Hummel, 2023, DOI: **10.1101/2023.10.11.554933**.
12 M. J. Wessel, E. Beanato, T. Popa, F. Windel, P. Vassiliadis, P. Menoud, V. Beliaeva, I. R. Violante, H. Abderrahmane, P. Dzialecka, C.-H. Park, P. Maceira-Elvira, T. Morishita, A. M. Cassara, M. Steiner, N. Grossman, E. Neufeld and F. C. Hummel, *Nat. Neurosci.*, 2023, **26**(11), 2005–2016.
13 P. Vassiliadis, E. Beanato, T. Popa, F. Windel, T. Morishita, E. Neufeld, J. Duque, G. Derosiere, M. J. Wessel and F. C. Hummel, *Nat. Hum. Behav.*, 2024, DOI: **10.1038/s41562-024-01901-z**.
14 M. Bikson, M. Inoue, H. Akiyama, J. K. Deans, J. E. Fox, H. Miyakawa and J. G. R. Jefferys, *J. Physiol.*, 2004, **557**, 175–190.
15 J. K. Deans, A. D. Powell and J. G. R. Jefferys, *J. Physiol.*, 2007, **583**, 555–565.
16 F. Karimi, A. Attarpour, R. Amirfattahi and A. Z. Nezhad, *Phys. Med. Biol.*, 2019, **64**, 235010.
17 S. Ghosh, A. K. Bera and S. Das, *J. Theor. Biol.*, 1999, **200**, 299–305.
18 L. Mosgaard, K. Zecchi, T. Heimburg and R. Budvytyte, *Membranes*, 2015, **5**, 495–512.
19 L. D. Mosgaard, K. A. Zecchi and T. Heimburg, *Soft Matter*, 2015, **11**, 7899–7910.
20 T. Heimburg, *Biophys. J.*, 2012, **103**, 918–929.
21 N. Grossman, M. S. Okun and E. S. Boyden, *JAMA Neurol.*, 2018, **75**, 1307.
22 W. Guo, Y. He, W. Zhang, Y. Sun, J. Wang, S. Liu and D. Ming, *Front. Neurosci.*, 2023, **17**, 1092539.
23 E. Mirzakhalili, B. Barra, M. Capogrosso and S. F. Lempka, *Cell Syst.*, 2020, **11**, 557–572.e5.
24 A. Opitz and W. J. Tyler, *Nat. Biomed. Eng.*, 2017, **1**, 632–633.
25 S. Rampersad, B. Roig-Solvas, M. Yarossi, P. P. Kulkarni, E. Santarnecchi, A. D. Dorval and D. H. Brooks, *NeuroImage*, 2019, **202**, 116124.
26 X. Song, X. Zhao, X. Li, S. Liu and D. Ming, *J. Neural Eng.*, 2021, **18**, 036003.
27 Z. Zhu and L. Yin, *Front. Hum. Neurosci.*, 2023, **17**, 1266753.
28 S. Bahn, C. Lee and B. Kang, *Hum. Brain Mapp.*, 2023, **44**, 1829–1845.
29 S. Lee, J. Park, D. S. Choi, C. Lee and C.-H. Im, *Comput. Biol. Med.*, 2022, **143**, 105337.
30 S. Lee, J. Park, D. S. Choi, S. Lim, Y. Kwak, D. P. Jang, D. H. Kim, H. B. Ji, Y. B. Choy and C.-H. Im, *J. Neural Eng.*, 2022, **19**, 056003.
31 S. Lee, C. Lee, J. Park and C.-H. Im, *Sci. Rep.*, 2020, **10**, 11730.
32 V. G. Carmona-Barrón, I. S. F. Del Campo, J. M. Delgado-García, A. J. De La Fuente, I. P. Lopez and M. A. Merchán, *Front. Neuroanat.*, 2023, **17**, 1128193.
33 Z. Zhu, Y. Xiong, Y. Chen, Y. Jiang, Z. Qian, J. Lu, Y. Liu and J. Zhuang, *Neural Plast.*, 2022, **2022**, 1–7.
34 C. Thomas, P. Springer, G. Loeb, Y. Berwaldnetter and L. Okun, *Exp. Cell Res.*, 1972, **74**, 61–66.
35 A. Ahtiainen, B. Genocchi, J. M. A. Tanskanen, M. T. Barros, J. A. K. Hyttinen and K. Lenk, *Int. J. Mol. Sci.*, 2021, **22**, 12770.
36 A. Ahtiainen, I. Annala, M. Rosenholm, S. Kohtala, J. Hyttinen, J. M. A. Tanskanen and T. Rantamäki, *Neuropharmacology*, 2023, **229**, 109481.
37 F. J. Chaure, H. G. Rey and R. Q. Quiroga, *J. Neurophysiol.*, 2018, **120**, 1859–1871.
38 F. E. Kapucu, J. M. A. Tanskanen, J. E. Mikkonen, L. Ylä-Outinen, S. Narkilahti and J. A. K. Hyttinen, *Front. Comput. Neurosci.*, 2012, **6**, 38.
39 I. A. Välkki, K. Lenk, J. E. Mikkonen, F. E. Kapucu and J. A. K. Hyttinen, *Front. Comput. Neurosci.*, 2017, **11**, 40.
40 P. Welch, *IEEE Trans. Audio Electroacoust.*, 1967, **15**, 70–73.
41 F. E. Kapucu, I. Välkki, J. E. Mikkonen, C. Leone, K. Lenk, J. M. A. Tanskanen and J. A. K. Hyttinen, *Front. Comput. Neurosci.*, 2016, **10**, 112.
42 Z. Esmaeilpour, G. Kronberg, D. Reato, L. C. Parra and M. Bikson, *Brain Stimul.*, 2021, **14**, 55–65.

43 X. Su, J. Guo, M. Zhou, J. Chen, L. Li, Y. Chen, X. Sui, H. Li and X. Chai, *IEEE Trans. Neural Syst. Rehabil. Eng.*, 2021, **29**, 418–428.
44 E. Acerbo, A. Jegou, C. Luff, P. Dzialecka, B. Botzanowski, F. Missey, I. Ngom, S. Lagarde, F. Bartolomei, A. Cassara, E. Neufeld, V. Jirsa, R. Carron, N. Grossman and A. Williamson, *Front. Neurosci.*, 2022, **16**, 945221.
45 Y. Huang, A. A. Liu, B. Lafon, D. Friedman, M. Dayan, X. Wang, M. Bikson, W. K. Doyle, O. Devinsky and L. C. Parra, *eLife*, 2017, **6**, e18834.
46 C. Ineichen, N. R. Shepherd and O. Sürücü, *Front. Hum. Neurosci.*, 2018, **12**, 468.
47 D. A. Wagenaar, J. Pine and S. M. Potter, *BMC Neurosci.*, 2006, **7**, 11.
48 T. Hyvärinen, A. Hyysalo, F. E. Kapucu, L. Aarnos, A. Vinogradov, S. J. Eglen, L. Ylä-Outinen and S. Narkilahti, *Sci. Rep.*, 2019, **9**, 17125.
49 F. H. Kasten, J. Dowsett and C. S. Herrmann, *Front. Hum. Neurosci.*, 2016, **10**, 245.
50 T. Neuling, S. Rach and C. S. Herrmann, *Front. Hum. Neurosci.*, 2013, **7**, 161.
51 B. C. Albensi, D. R. Oliver, J. Toupin and G. Odero, *Exp. Neurol.*, 2007, **204**, 1–13.
52 S. Ahn, S. Jo, S. B. Jun, H. W. Lee and S. Lee, *Front. Comput. Neurosci.*, 2017, **11**, 39.
53 S.-N. Lim, C.-Y. Lee, S.-T. Lee, P.-H. Tu, B.-L. Chang, C.-H. Lee, M.-Y. Cheng, C.-W. Chang, W.-E. J. Tseng, H.-Y. Hsieh, H.-I. Chiang and T. Wu, *Neuromodulation*, 2016, **19**, 365–372.
54 E. Paschen, C. Elgueta, K. Heining, D. M. Vieira, P. Kleis, C. Orcinha, U. Häussler, M. Bartos, U. Egert, P. Janz and C. A. Haas, *eLife*, 2020, **9**, e54518.
55 Y. Schiller and Y. Bankirer, *J. Neurophysiol.*, 2007, **97**, 1887–1902.
56 W. Singer, *Neuron*, 1999, **24**, 49–65.
57 T. P. Vogels and L. F. Abbott, *J. Neurosci.*, 2005, **25**, 10786–10795.
58 M. Diesmann, M.-O. Gewaltig and A. Aertsen, *Nature*, 1999, **402**, 529–533.